NUMERICAL GRID GENERATION
Joe F. Thompson, editor



# CONFORMAL GRID GENERATION FOR MULTIELEMENT AIRFOILS*

DOUGLAS HALSEY+
+Aerodynamics Research Department, Douglas Aircraft Company, 3855 Lakewood Blvd., Long Beach, California, 90846 USA

## INTRODUCTION

Conformal mapping provides an effective means of generating suitable grids for use in the numerical solution of many two-dimensional flow problems. There are numerous examples of its use for problems involving single-element airfoils, including the well-known finite-difference transonic flow codes of Garabedian and Korn[1] and Jameson[2]. The present author[3] has found conformal mapping to be especially useful in computing compressible potential flow using an integral-equation (or field-panel) approach similar to that used by Wu and Thompson[4], Luu and Coulmy[5], and others. In this approach, a body is analyzed in an equivalent inviscid, incompressible flow with distributed singularities in the external field. The distribution of the singularities is determined in an iterative manner, using the fully nonlinear field equation, the computed flow field, and the appropriate solid-body boundary conditions. Application of a conformal mapping to this problem simply modifies the magnitudes of the singularity strengths and the boundary conditions, without changing the general form of either. The regular spacing in the transformed plane allows the application of very efficient numerical procedures which make effective use of the fast Fourier transform algorithm. For example, using the grid transformations shown in figure 1, accurate subsonic compressible flow solutions for single-element airfoil cases have been obtained in less than two seconds of CPU time on an IBM 370 computing system.

Conformal mapping has also been used for problems involving two-element airfoils. For example, the finite-difference transonic flow code developed by Grossman and Volpe[6] makes use of a mapping, developed by Ives[7], in which the region outside two airfoil elements is transformed to the annular region between two concentric circles. In that case, however, it was necessary to apply nonconformal shearing transformations to the resulting grids, in order

*This research was sponsored by the Independent Research and Development Program of the McDonnell-Douglas Corporation.

to obtain suitable point spacing distributions. This illustrates the unfortunate fact that conformal mapping methods do not allow the degree of control over grid point spacing offered by some other methods, such as the differential equation methods of Thompson[8].

Conformal mapping has not yet been used to generate grids for flow problems involving general multielement airfoils with more than two elements (at least, not to the author's knowledge). This development has been hindered by the absence of any suitable conformal mapping methods for general multielement airfoils. However, the recent development of such methods by the present author[9] and by Harrington[10] should result in the increased use of conformal mapping for multielement airfoil problems.

This paper describes recently-developed techniques applicable to cases involving general multielement airfoils having any number of airfoil elements. Each technique can be considered as a purely geometric construction or, equivalently, as a network of streamlines and potential-lines of an auxiliary potential-flow solution. The nonuniqueness of such solutions ensures the existence of a wide variety of conformal grid types, each having different point-spacing characteristics. A chronicle is given of the search for the type of grid most suitable for solving the inviscid compressible flow equations using a distributed-source field-panel approach. Examples are shown for grids involving up to four airfoil elements.

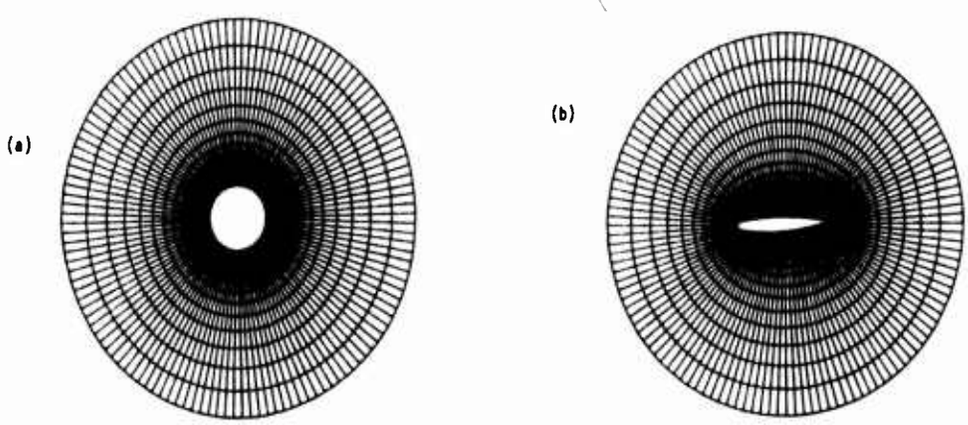


Fig. 1. Typical conformal grid for a single-element airfoil.
(a) Circle plane.
(b) Physical plane.

CONFORMAL MAPPING OF MULTIELEMENT AIRFOILS

A prerequisite for the development of conformal grid generation techniques for multielement airfoils is the existence of a method for transforming the multiple airfoil elements to a system of bodies having much simpler geometry. Such a method has been developed by the present author[9]. This method makes use of a succession of comparatively simple single-body transformations to solve the more difficult multiple-body problem. In the first step, a succession of inverse Karman-Trefftz mappings is applied. Each of these mappings removes a single corner (or a pair of corners in some cases) from a single body, and also causes smaller perturbations to the shapes of the other bodies. At the end of this step, there are no corners and, in most cases, all bodies are quasi-circular in shape. The next step is an iterated sequence of mappings, each of which maps a single body to a perfect circle, and also causes small perturbations to the other bodies. At the end of each iteration of this sequence, the final body is perfectly circular and the other bodies are more nearly circular than at the end of the previous iteration. Iterations proceed until all bodies are sufficiently close to perfect circles and the derivative of the mapping function converges to within a sufficiently small tolerance. Because of the rapid decay with distance of the effects of

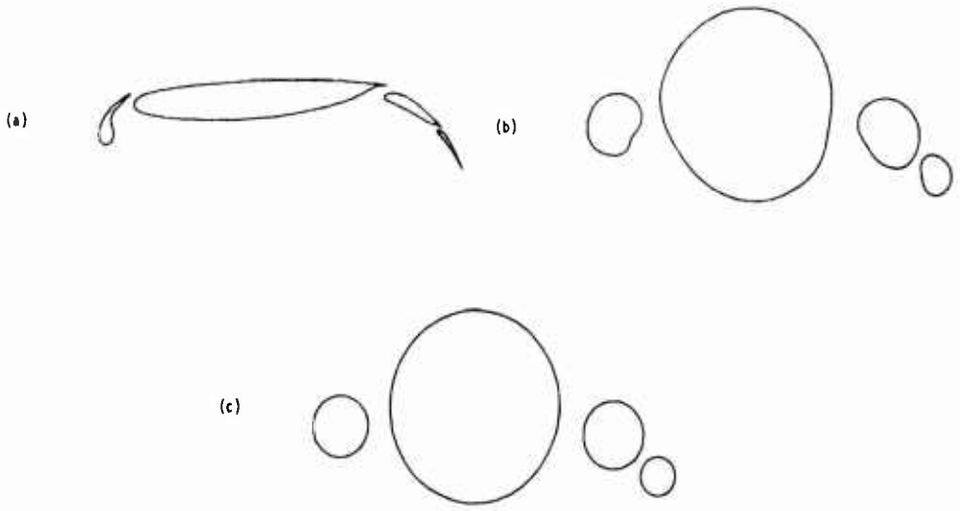


Fig. 2. Transformation of a four-element airfoil into four circles.
(a) Physical geometry.
(b) Geometry after four corner-removing mappings.
(c) Geometry after four circle mappings.

these mappings, the entire procedure converges extremely quickly. Three to five iterations are usually sufficient to give four-digit accuracy. The entire procedure usually requires less than three CPU seconds on an IBM 370 computer. This process is illustrated in figure 2, which shows a four-element airfoil, the geometry after the removal of all corners, and the geometry after only one iteration of the circle mappings. An extension of this procedure to allow airfoils with open trailing edges to be included is described in reference 11.

## GRIDS USING A STRING MAPPING

One straightforward grid generation procedure for multielement airfoils involves stringing the airfoil elements together into a single effective body, in a manner reminiscent of Thompson's treatment of multielement airfoils[8]. In this approach, it is not necessary to use a conformal mapping method for multielement airfoils, although the geometric problems are simplified somewhat if the bodies have been previously transformed to circles. This grid generation procedure requires the following steps: 1) String the bodies together into a single body and order the points in a continuous array around the perimeter of the effective body. 2) Apply the Karman-Trefftz transformation successively to remove the resulting corners in the effective body. 3) Transform the resulting body into a perfect circle. 4) Set up the grid in the circle plane. 5) Perform the transformations in reverse order, bringing the grid points back to the multiple-circle plane and finally back to the physical plane. The steps in this process are illustrated in figure 3 for a three-element airfoil case. For step 3, a very robust circle mapping method is necessary, since the shapes to be transformed are too complicated for more limited methods. A comparison of two alternative circle mapping methods is given in reference 12.

Grids produced by this technique for two- and three-element airfoil cases are illustrated in figure 4. These grids are very similar to single-element grids, such as the one illustrated in figure 1 and the flow calculation technique of reference 3 can be directly applied. Point density in these grids is suitably high near the leading edge of the forward element and the trailing edge of the aft element, but there are undesirable sparse areas between the airfoil elements. Although these sparse areas may not cause serious errors in some calculations, they clearly limit the general applicability of this grid generation technique.

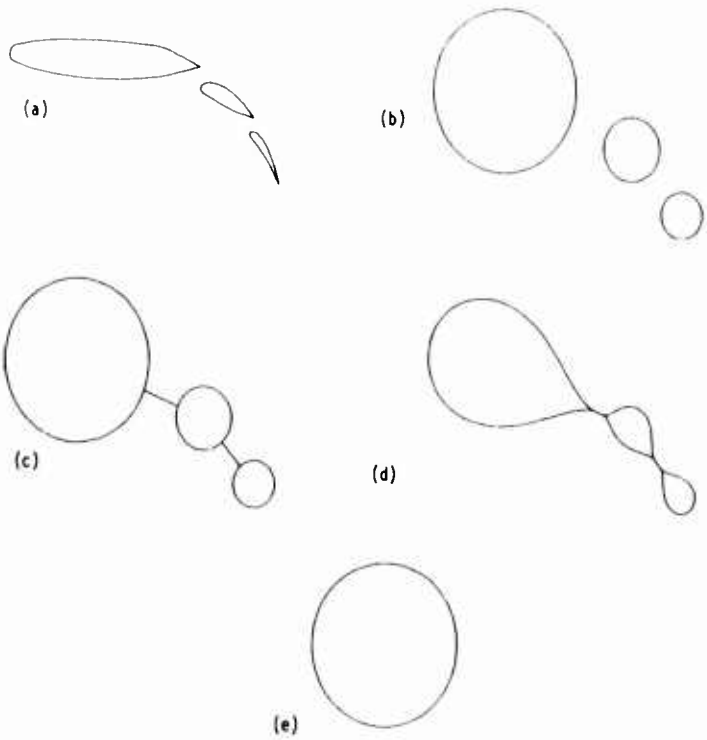


Fig. 3. "String mapping" for a three-element airfoil.
(a) Physical geometry.
(b) Geometry in multiple-circle plane.
(c) Single body produced by stringing circles together.
(d) Geometry after corner-removing mappings.
(e) Unit circle.

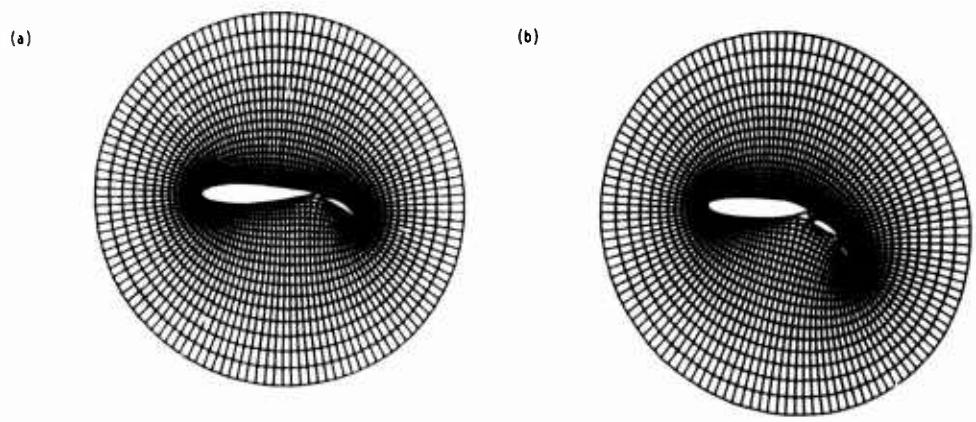


Fig. 4. Grids generated using the string mapping.
(a) Two-element airfoil.
(b) Three-element airfoil.

GRIDS USING STREAMLINE/POTENTIAL-LINE NETWORKS

The grids described above were derived using purely geometric conformal constructions. Other types of grids can be derived from networks of streamlines and potential-lines from auxiliary potential-flow solutions. These grids are conformal as a result of the fact that the complex potential ($\Phi = \phi + i\psi$, where $\phi$ and $\psi$ are the scalar potential and stream function) and the complex velocity are analytic functions of each other. In fact, any conformal grid can be considered to be a potential/stream-function network ($\phi$-$\psi$ grid for short) for some potential flow. In this context, the grids described in the above section can be derived from a flow with a point vortex at the center of the circle in the transformed plane. The nonuniqueness of the potential-flow problem for given geometry ensures that a wide variety of types of conformal grid can be constructed.

The development of a $\phi$-$\psi$ grid generation capability for multielement airfoils (using the present author's conformal mapping procedures) requires a method for computing the flow around the multiple circles, with constant stream function on each circle. Such a method is described in reference 9 and briefly below.

Any incompressible potential flow solution can be represented by a linear combination of simpler fundamental solutions. In the present method, there are two noncirculatory fundamental solutions and a number of circulatory solutions equal to the number of circles. Each noncirculatory solution has unit freestream and zero circulation about each circle. The two solutions have different angles of attack of the freestream flow. Each circulatory solution has zero freestream, unit circulation about one circle, and zero circulation about all other circles. The two noncirculatory solutions and one of the circulatory solutions for a three-circle case are illustrated in figure 5.

The calculation of each noncirculatory flow solution involves finding an infinite sequence of reflected point doublet singularities within the circles. Each circulatory flow solution involves finding a similar infinite sequence of point vortex singularities. The result of each flow solution is a series expansion for the complex velocity as a function of complex coordinate. This is easily converted to a series for the complex potential having the following form:

$$(\phi+i\psi) = \sum_{NB=1}^{NBDS} \{a_{0_{NB}} (\zeta-\zeta_{NB}) + a_{1_{NB}} \log(\zeta-\zeta_{NB}) + a_{2_{NB}} (\zeta-\zeta_{NB})^{-1} + a_{3_{NB}} (\zeta-\zeta_{NB})^{-2} + \ldots \} \qquad (1)$$

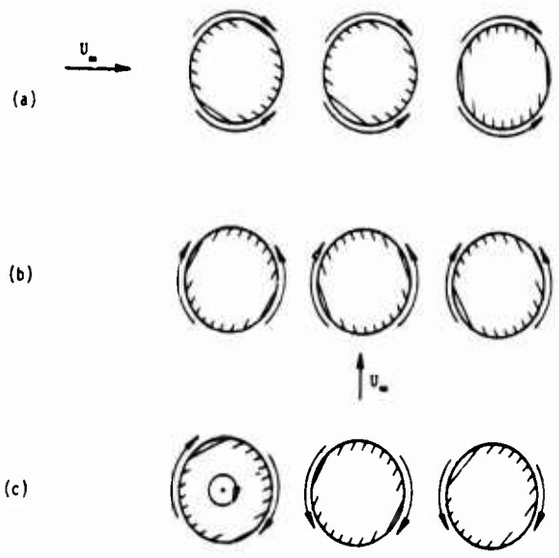


Fig. 5. Nonuniqueness of potential-flow solutions.
(a) Noncirculatory flow with freestream at $\alpha = 0°$.
(b) Noncirculatory flow with freestream at $\alpha = 90°$.
(c) Circulatory flow with stagnant freestream.

where $\zeta$ is the complex coordinate of the point at which the flow is to be computed, $\zeta_{NB}$ is the complex coordinate of the center of the circle having index NB, NBDS is the total number of circles, and the series coefficients $(a_{ij})$ are generally complex.

The calculation procedure for each point in a $\phi$-$\psi$ grid consists of solving equation (1) for the complex coordinate corresponding to the specified value of the complex potential in the multiple-circle plane, followed by a transformation to determine the complex coordinate in the physical plane. The solution of equation (1) is accomplished by a Newton iteration procedure for nonlinear complex equations. Having solved equation (1) on the boundaries of a region of the flow, the solution in the interior can often be obtained more efficiently using a fast Laplace solver.

## $\phi$-$\psi$ grids for streaming flows

The most common flow solutions used for producing $\phi$-$\psi$ grids are probably the standard streaming flows, with uniform freestream and smooth flow off the trailing edge of each airfoil element. These can be obtained by combining all the fundamental flows described in the previous section. The combination constants for the noncirculatory fundamental flows depend only on the flow

angle of attack. The combination constants for the circulatory solutions are found by imposing the Kutta condition at the trailing edge of each airfoil element. In the multiple-circle plane, this requires specifying zero tangential velocity component at the images of the trailing-edge points and solving the resulting set of linear equations.

The point spacing in the physical plane of a $\phi$-$\psi$ grid is inversely proportional to the local flow speed. Consequently, a grid around a body which causes only a small perturbation to a uniform flow should have nearly uniform spacing. This is illustrated in figure 6(a), which shows a grid for a single-element airfoil at a small angle of attack. Flow solutions with extensive low-speed regions have extensive sparse areas. This is illustrated in figure 6(b), which shows a grid around two circles, with large sparse areas near the leading- and trailing-edge stagnation points.

These grids are divided into a number of segments, separated by the stagnation streamlines. Within each segment, increments of stream function and potential are constant, resulting in a rectangular grid in the $\phi$-$\psi$ plane. A logarithmic mapping transforms the rectangular region into an annular one similar to figure 1(a). The efficient flow calculation techniques of reference 3 can then be used to find the influence of each region at points in all the regions.

For the present application, these grids have several drawbacks. First, the sparse areas near the leading edges would give inadequate definition of the rapidly-varying field-source density. Second, the uniformly-spaced areas far from the bodies would reduce the solution efficiency by adding unnecessary points. Third, the flow calculation procedure of reference 3 is most efficient if O-type grids can be used.

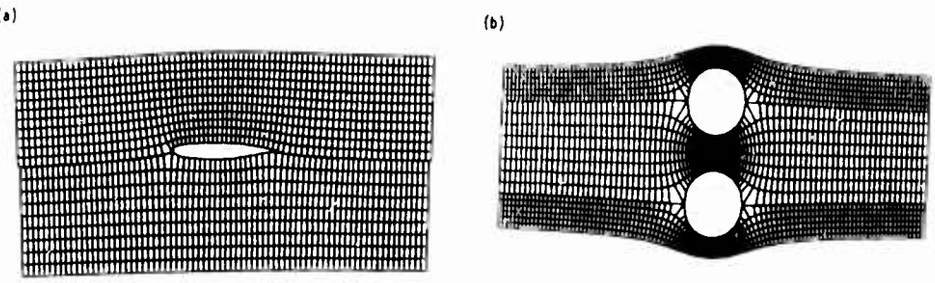


Fig. 6. Grids derived from potential-flow solutions for streaming flows.
(a) Single-element airfoil.
(b) Two circles.

## $\phi$-$\psi$ grids for circulatory fundamental flows

O-type grids can be obtained from $\phi$-$\psi$ networks if flow solutions having circulation but no freestream are used. The point vortex solution for single-element cases, mentioned earlier, is an example of such an application. The simplest multielement flow solutions having circulation but no freestream are the circulatory fundamental flow solutions, having unit circulation about one body and zero circulation about all others. Like the $\phi$-$\psi$ grids for streaming flows, these grids are divided into a number of segments by the stagnation streamlines. In each segment, the increments in stream function and potential are constant and the flow calculation procedure is identical to that for a $\phi$-$\psi$ grid for a streaming flow.

Examples of circulatory $\phi$-$\psi$ grids are shown in figure 7 for two- and three-element airfoil cases. In general, the point distribution around the circulatory body is very desirable, with high point density near the leading and trailing edges and lower point density near mid-chord. The noncirculatory bodies have high point density near the leading and trailing edges, but they have far too low point density near the stagnation points on the upper and lower surfaces. Grids of this type would probably only be suitable for cases in which the expected flow solution is rapidly varying on just one of the airfoil elements.

## $\phi$-$\psi$ grids for more general flows

The most undesirable features of the $\phi$-$\psi$ grids discussed above are the sparse areas associated with stagnation points on the bodies. In many cases,

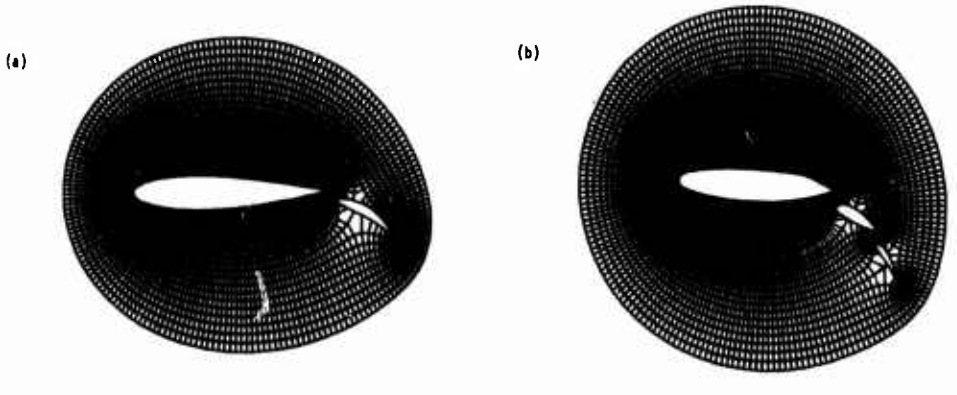


Fig. 7. Grids derived from potential-flow solution for circulatory fundamental flows.
(a) Two-element airfoil.
(b) Three-element airfoil.

however, it is possible to eliminate stagnation points entirely or move them so far from the bodies as to be inconsequential. One strategy for accomplishing this is to combine circulatory fundamental flows, alternate the sign of the circulation on adjacent bodies, and adjust the magnitudes to make the total circulation equal zero. Examples of portions of grids of this type are illustrated in figure 8. The most obvious feature of these grids is their extremely high point density in the areas between the bodies which, for a given total number of points causes sparse areas elsewhere. Another feature is that each grid is divided into a number of segments, within each of which the streamlines circulate around a single body. The dividing streamlines between the segments extend to infinity in both directions. Both of these features are undesirable for the present flow computation procedure, prompting the search for still further types of conformal grids.

One way of eliminating the infinite extent of the grid and also changing the point distribution is to allow the total circulation to be nonzero. At some distance from the bodies, the streamlines will then circulate around all the bodies and the grid can be truncated at any one of these streamlines. Spacing problems still remain, however, and can even become more serious as new stagnation points arise in the flow.

More control of the spacing can be obtained by introducing fictitious bodies or singularities into the flow (out of the range covered by the grid). If a new body surrounds all the other bodies and contains the entire flow in its interior, control is also achieved over the extent of the grid. This has

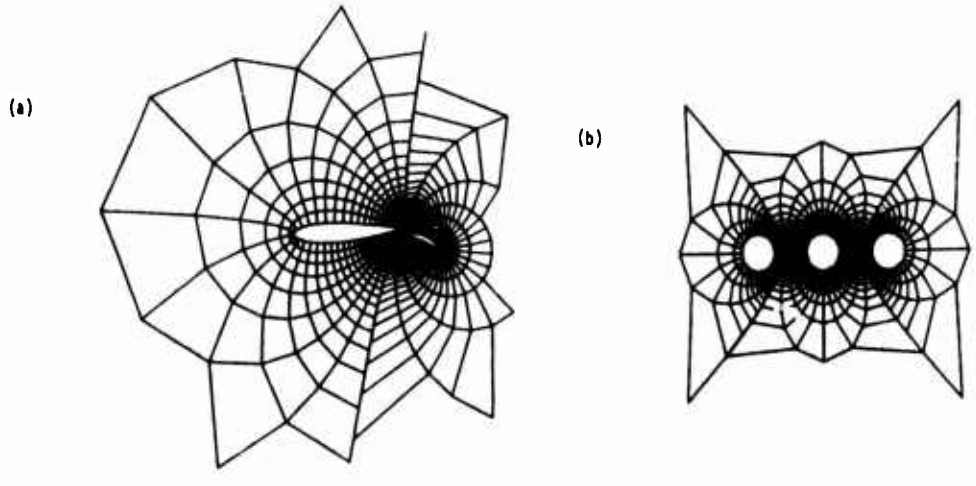


Fig. 8. Grids derived from potential-flow solutions for more general flows (zero total circulation).

been implemented by adding a larger circle around the original bodies in the multiple-circle plane. Calculation procedures for the auxiliary potential flow are only slightly modified by this addition, requiring the series for the complex potential to include positive as well as negative powers of the complex coordinate. An example of a portion of a grid generated in this manner is shown in figure 9. This is a big improvement over the previous grids; the point spacing is more appropriate and the grid extent is now finite.

Flow calculations using any of the grids discussed in this section encounter difficulties not found when any of the previous grids are used. The efficient flow calculation procedures of reference 3 can still be used to find the influence of the singularities within any given grid segment at points within that same segment, but they can no longer be used directly to find the influence at points outside the given segment. This is because the segment boundaries now represent folds in a Riemann surface, rather than just discontinuities in point spacing. Another way of expressing this is to note that the stream function is not a monotonic function of distance along any line crossing the dividing streamlines and, as a result, two or more points in different segments of a grid can have identical values of the complex potential.

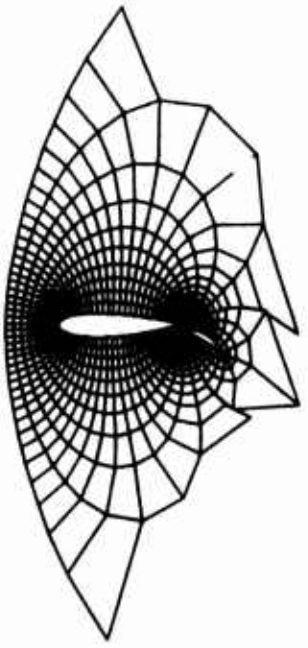

Fig. 9. Grid derived from a potential-flow solution for a more general flow (nonzero circulation and fictitious body).

These grids can still be very useful, especially in a field-panel method, but means of communication between the segments must be developed. These techniques could be very similar to the flow segmentation techniques described by Wu[13], et al. Given the influence of a segment on its boundaries, the influence at exterior points can be computed using either boundary singularities or a fast Laplace solver (perhaps with the aid of additional transformations). The details of these segment communication techniques have yet to be worked out.

## SEGMENTED GRIDS WITH SPECIFIED BOUNDARIES

A greater degree of grid control can be achieved by directly specifying the shapes of the region boundaries, rather than using whatever shapes the dividing streamlines of a flow solution may form. In order to force the boundaries to be streamlines of the flow, it is necessary to distribute vortex singularities on the boundaries. The distribution of these singularities could be computed using a boundary-integral-equation technique similar to the panel methods for aerodynamic analysis developed by Hess[14] and others. A more efficient computational approach makes further use of conformal mapping. In this approach, each segment of the grid is dealt with independently of the other segments. The region between a single element of the multielement airfoil system and the boundary surrounding it is transformed to the annular region between two concentric circles. A polar grid in each annular segment is constructed and transformed back to the physical plane. The resulting grid is equivalent to the $\phi$-$\psi$ grid which would be computed using the vortex singularity approach.

The process of transforming a given region to an annulus is very similar to the method for transforming a multielement airfoil to a system of multiple circles. The first step is to apply a sequence of inverse Karman-Trefftz mappings, each of which removes a single corner from one of the boundaries. (If the boundary specification is performed in the multiple-circle plane, only the outer boundary will have any corners.) The next step is to apply an iterated sequence of mappings, each of which maps either the inner or the outer boundary to a perfect circle. In order to avoid the necessity of applying an interior mapping to the outer boundary and an exterior mapping to the inner boundary, an inversion mapping is performed after each circle mapping. At the end of a small number of iterations (typically three or four), both inner and outer boundaries are sufficiently close to circular and the derivative of the mapping function converges to within a small tolerance. Since these circles

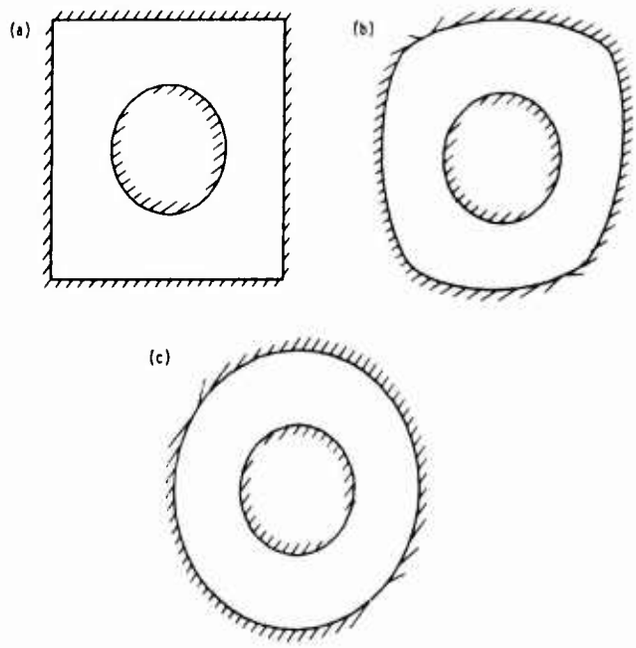


Fig. 10. Transformation to an annular region.
(a) Original geometry.
(b) Geometry after four corner-removing mappings.
(c) Geometry after two circle mappings and two inversions.

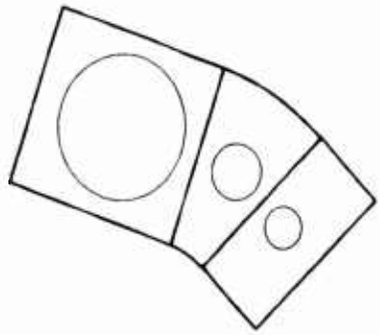

Fig. 11. Boundary construction for a segmented grid.

may not be concentric, it is necessary to perform a final linear fractional mapping. The steps of this transformation procedure are illustrated in figure 10 for one of the segments of the three-circle case shown in figure 11. An alternative approach to the annular mapping problem has been described by Ives[7]. Since his method is noniterative (except for the single-body mappings) it is perhaps more efficient. However, the present method can use simpler functions and the overall procedure is only slightly more expensive than computing two independent single-body mappings.

Grids produced by this technique for two- and three-element cases are shown in figure 12. In each case, a simple construction of straight lines and/or circular arcs in the multiple-circle plane was used to define the region boundaries. Point spacing around each airfoil element is similar to the spacing around the single-element airfoil of figure 1, with high point density at leading and trailing edges and no glaring sparse areas on the airfoil surfaces. Possible drawbacks of these grids include the presence of sparse areas near the corners of the outer boundaries and the necessity to locate boundaries too near the airfoil surfaces. (Moving the boundaries too far away produces sparse spacing on the airfoil surfaces.)

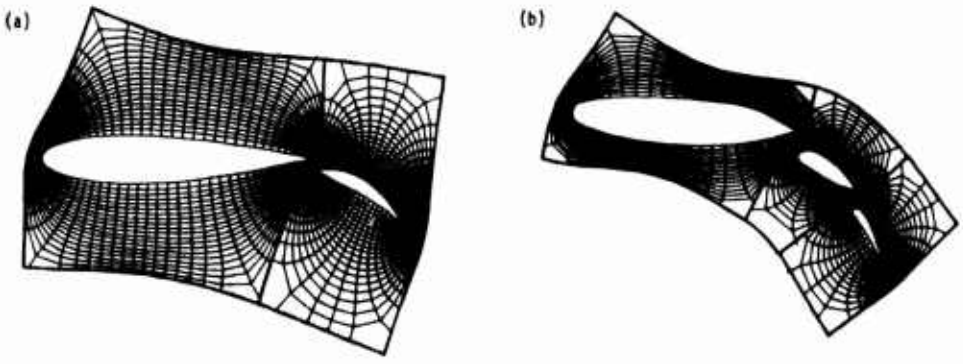


Fig. 12. Grids generated using the annular mapping.
(a) Two-element airfoil.
(b) Three-element airfoil.

HYBRID GRIDS

Improved grids can be obtained by combining the method described above with the string mapping illustrated earlier (figures 3 and 4). Instead of specifying the region boundaries arbitrarily, use can be made of curves generated using the string mapping. Region boundaries can be constructed using any of the curves surrounding all airfoil elements, together with sets of curves which run between the airfoil elements. In this way, two of the four corners (and their corresponding sparse areas) on the outer boundaries of the grid segments associated with the forward and aft airfoil elements are eliminated. It is also possible to extend the grid as far from the airfoil system as desired, by using a portion of the string grid directly in this region.

Grids produced by this technique for two-, three- and four-element cases are illustrated in figure 13. These grids retain the desirable features of the grids of figure 12, while eliminating most of their drawbacks.

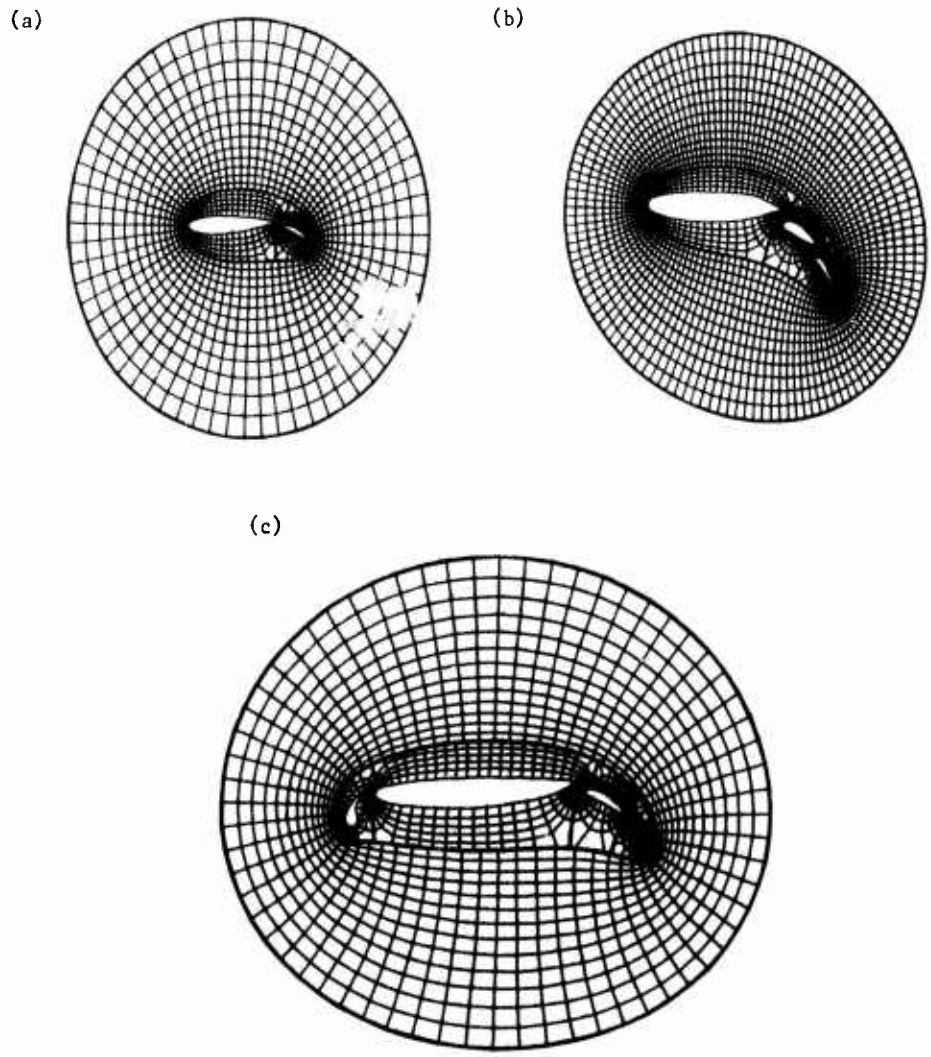


Fig. 13. Hybrid grids generated using both annular and string mappings.
(a) Two-element airfoil.
(b) Three-element airfoil.
(c) Four-element airfoil.

## CONCLUSIONS

A chronicle has been given of the search for the type of conformal grid most suitable for use in computing the inviscid compressible flow around multielement airfoils using a distributed-source field-panel approach. Although many of the grids were deemed not suitable for this application, they were included in order to illustrate the great diversity of types of conformal grid which can be constructed. The final grids, for the most part, have

desirable point distributions around each airfoil element, of a form to which the efficient flow analysis techniques developed earlier can be readily applied. They are possibly close to the best which can be derived without sacrificing the conformality properties.

ACKNOWLEDGMENT

The author has benefitted considerably from numerous discussions of conformal mapping and grid-generation techniques with his colleague at Douglas Aircraft Company, Dr. R. W. Clark.

REFERENCES

1. Garabedian, P. and Korn, D. (1971) Comm. P. & Appl. Math, XXIV.
2. Jameson, A. (1971) Grumman Report 390-71-1.
3. Halsey, D. (1981) Proceed. of the Symposium on Numerical Boundary Condition Procedures, NASA CP-2201, pp. 61-71.
4. Wu, J.C. and Thompson, J.F. (1973) Computers and Fluids, 1, 2, pp. 197-215.
5. Luu, T.S. and Coulmy, G. (1977) Computers and Fluids, 5, 4, pp. 261-275.
6. Grossman, B. and Volpe, G. (1977) Office of Naval Research Report ONR-CR215-241-1.
7. Ives, D.C. (1975) AIAA Paper 75-842.
8. Thompson, J.F. (1978) Lecture Series in Computational Fluid Dynamics, Von Karman Inst. for Fluid Dynamics, Belgium.
9. Halsey, N.D. (1979) AIAA Paper No. 79-0271, also AIAA J., 17, 12.
10. Harrington, A. To appear in Journal d'Analyse Mathematique.
11. Halsey, N.D. (1980) AIAA Paper No. 80-0069.
12. Halsey, N.D. To appear in AIAA J.
13. Wu, J.C., Spring, A.H., and Sankar, N.L. (1975) Lecture Notes in Physics - Proceedings of the Fourth International Conference on Numerical Methods in Fluid Dynamics, 35, pp. 452-457.
14. Hess, J.L. (1975) Computer Methods in Applied Mechanics and Engineering, 5, pp. 145-196.